NeuroImage 199 (2019) 570–584

Contents lists available at ScienceDirect

NeuroImage

journal homepage: www.elsevier.com/locate/neuroimage

In vivo widefield calcium imaging of the mouse cortex for analysis of network connectivity in health and brain disease

Julia V. Cramer [a,1], Benno Gesierich [a,1], Stefan Roth [a], Martin Dichgans [a,b], Marco Düring [a,*,1], Arthur Liesz [a,b,*,1]

[a] Institute for Stroke and Dementia Research, University Hospital, LMU Munich, Munich, Germany
[b] Munich Cluster for Systems Neurology (SyNergy), 80336, Munich, Germany

ARTICLE INFO

Keywords:
In vivo imaging
Mouse models
Neuronal network connectivity
Stroke
Recovery
ICA

ABSTRACT

The organization of brain areas in functionally connected networks, their dynamic changes, and perturbations in disease states are subject of extensive investigations. Research on functional networks in humans predominantly uses functional magnetic resonance imaging (fMRI). However, adopting fMRI and other functional imaging methods to mice, the most widely used model to study brain physiology and disease, poses major technical challenges and faces important limitations. Hence, there is great demand for alternative imaging modalities for network characterization. Here, we present a refined protocol for *in vivo* widefield calcium imaging of both cerebral hemispheres in mice expressing a calcium sensor in excitatory neurons. We implemented a stringent protocol for minimizing anesthesia and excluding movement artifacts which both imposed problems in previous approaches. We further adopted a method for unbiased identification of functional cortical areas using independent component analysis (ICA) on resting-state imaging data. Biological relevance of identified components was confirmed using stimulus-dependent cortical activation. To explore this novel approach in a model of focal brain injury, we induced photothrombotic lesions of the motor cortex, determined changes in inter- and intrahemispheric connectivity at multiple time points up to 56 days post-stroke and correlated them with behavioral deficits. We observed a severe loss in interhemispheric connectivity after stroke, which was partially restored in the chronic phase and associated with corresponding behavioral motor deficits. Taken together, we present an improved widefield calcium imaging tool accounting for anesthesia and movement artifacts, adopting an advanced analysis pipeline based on human fMRI algorithms and with superior sensitivity to recovery mechanisms in mouse models compared to behavioral tests. This tool will enable new studies on interhemispheric connectivity in murine models with comparability to human imaging studies for a wide spectrum of neuroscience applications in health and disease.

1. Introduction

Functional brain networks and their alterations are of great interest for understanding mechanisms in health and neurological diseases. Connectivity analysis based on functional magnetic resonance imaging (fMRI) in humans has facilitated our growing understanding of physiological and pathological processes in the brain. However, mechanistic studies, identification of novel therapeutic targets and drug development are mostly conducted in mouse models. These models allow genetic modifications, in depth analysis of biological samples and pharmacological testing, which is driving translational sciences. To improve comparability of translational neuroscience research to findings in humans, development of brain network analysis in mice is necessary. Yet, fMRI analysis is very challenging and limited in mice, due to their size and long procedure times often combined with intravenous anesthesia and intubation (Schroeter et al., 2014; Zerbi et al., 2015). Additionally, fMRI analysis is based on blood oxygenation levels, allowing only indirect measurements of neural activity. Therefore, our aim was to establish an imaging approach that would circumvent these limitations while maintaining the comparability of the analysis approaches to human fMRI.

For this reason, we adapted *in vivo* widefield calcium imaging of

* Corresponding authors. Institute for Stroke and Dementia Research, Klinikum der Universität München, Feodor-Lynen-Straße 17, 81377, Munich, Germany.
E-mail addresses: marco.duering@med.uni-muenchen.de (M. Düring), arthur.liesz@med.uni-muenchen.de (A. Liesz).
[1] these authors contributed equally, respectively.

https://doi.org/10.1016/j.neuroimage.2019.06.014
Received 3 November 2018; Received in revised form 27 May 2019; Accepted 4 June 2019
Available online 7 June 2019

neuronal activity (Kozberg et al., 2016; Ma et al., n.d.; Matsui et al., 2016; Silasi et al., 2016; Vanni and Murphy, 2014; Wright et al., 2017) as a reversed translational approach from bedside to bench. We used Thy1GCaMP6s heterozygous mice, which express genetically-encoded calcium indicators (GECIs). The GECI expressed in these animals is a calmodulin-bound green fluorescent protein (GCaMP), which increases fluorescence at high intracellular calcium levels. The Thy1 promotor is limiting the GCaMP expression specifically to excitatory neurons, predominantly in layer 5 as well as layer 2 and 3 pyramidal cells (Dana et al., 2014). Hence, fluorescence intensity recorded from these mice directly mirrors cortical neuronal activity. This method not only allows repetitive, non-invasive measurements but is also blood flow-independent. This is mandatory to reduce interference of possible pathological changes in neurovascular coupling, which is understood to play a pivotal role in several brain diseases (Iadecola, 2004). Using this widefield imaging approach, we were able to repetitively acquire both spontaneous resting-state and stimulus-dependent activity from both forebrain hemispheres in healthy mice and after experimental stroke induction. We then used analysis algorithms comparable to the ones commonly used in fMRI analysis in order to generate a truly translational research tool.

Compared to previous attempts of establishing such a method, we advanced the sedation protocols to avoid anesthesia-associated bias and used objective measures to control for anesthesia artifacts. We introduced a procedure to register brains spatially between different recordings within the same mouse and between different mice and thereby ensured inter- and intra-subject comparability – a prerequisite for reliable group analysis. Furthermore, we implemented advanced analytical paradigms to neuronal calcium-imaging, such as the use of independent component analysis (ICA) for functional network characterization.

Finally, we wanted to examine the performance of this procedure by investigating changes in functional connectivity in a disease model. We chose to explore the impact of acute stroke on cortical networks. Stroke is a paradigmatic disease for acute brain injury which in addition is one of the leading causes of morbidity in industrialized countries. Hence, tools to study recovery mechanisms after stroke are urgently sought after. A new imaging modality with broader applicability in rodents than fMRI might facilitate novel avenues of research on recovery after stroke. We applied this optimized method to investigate post-stroke dynamic changes of functional connectivity as a hallmark of post-stroke brain injury and regeneration. Previous studies using fMRI in humans have advanced our knowledge about neuronal plasticity and recovery after stroke (Silasi and Murphy, 2014). Not only the changes in functional networks in the brain during acute and chronic stroke but also their influence on motoric rehabilitation have been well studied (Cramer et al., 1997; Grefkes and Fink, 2011), linking functional network connectivity to stroke outcome (Carter et al., 2012, 2010; Urbin et al., 2014). In our model, we specifically targeted the motor cortex in mice by using a photothrombotic stroke model and repetitively imaged animals during their recovery up to 2 months after stroke. We discovered desynchronisation of interhemispheric homotypic areas and partial restoration of network function in the chronic phases after stroke. Hence, we provide evidence for the applicability of an advanced calcium-dependent imaging modality of neuronal activity of nearly the entire forebrain cortex in mice and its feasibility for investigating the integrity and pathological/adaptive changes of functional cortical networks in acute and chronic brain diseases.

2. Material and methods

2.1. Sub-studies: the anesthesia, network and stroke study

This study consisted of three sub-studies. In a first study (further called anesthesia study), three different anesthesia protocols were tested (1.5% ISO, 1.0% ISO, MED + ISO; n = 9), in order to select a protocol providing as-low-as-possible and consistent levels of anesthesia depth across animals and days. Also, the effect of each anesthesia protocol on functional connectivity was assessed.

In a second study (further called network study), ICA (in particular an extension of classical ICA called independent vector analysis (IVA)) was used to define distinct functional cortical networks on resting-state acquisitions (n = 41–47). Somatosensory stimulation (n = 23) was further used to identify the functional involvement of the different IVA derived networks. Regions of interest (ROI) were derived from the peak pixel of the areas being part of the independent component spatial maps.

In a third study (further called stroke study), the established anesthesia protocol and ROI were used to assess pathological changes and recovery of functional connectivity after an acute injury (i.e. photothrombosis) to the motor cortex (sham n = 17; stroke n = 23). This experiment was conducted in a total of 7 subgroups of mice, from which all were followed up until day 28 and only the final two groups until day 56 after stroke. This last study was meant to support the concept that our new paradigm can be a valuable approach in the study of disease models.

2.2. Animals

All experiments were conducted in accordance with national guidelines for the use of experimental animals and all protocols were approved by the German governmental committees (Regierung von Oberbayern, Munich, Germany). C57BL/6J-Tg(Thy1-GCaMP6s)GP4.12Dkim/J (Dana et al., 2014) heterozygous mice were bred at the Institute for Stroke and Dementia Research, Munich. The Thy1 promotor is limiting the GCaMP expression specifically to excitatory neurons, predominantly in layer 5 as well as layer 2 and 3 pyramidal cells (Suppl. Fig. 1). Mice were housed at controlled temperature (22 ± 2 °C), with a 12-h light–dark cycle period and had access to pelleted food and water ad libitum. Both male and female animals were used for this study at 12–15 weeks of age due to full-grown size of the skull at this age. During all anesthetized procedures body temperature was maintained using a feedback-controlled heating system. After end of anesthesia animals were put in a heating chamber until they recovered from anesthesia.

2.3. Skull preparation

Skull preparation was performed using a modified version of the previously published protocol of Silasi et al. (2016). Briefly, after induction of anesthesia mice were placed into a stereotactic frame (product no.: 51501, Stoelting, Europe). The head was fixed, scalped and the underlying connective tissue was gently removed. After cleaning and disinfection, a layer of transparent dental cement (Quick Base S398, L-Powder clear S399, Universal Catalyst S371, Parkell C&B metabond, USA) was applied and covered with a tailored coverslip (24 × 60mm #1, 5, Menzel-Gläser, Germany). The mice stayed anesthetized until the cement was dried and were afterwards allowed to recover for more than 48 h before the first image acquisition. Two mice (one in stroke, one in sham group) removed their cranial windows (after 5 and 42 days, respectively) and were consequently excluded from further recordings.

2.4. Anesthesia

In a first study three different anesthesia protocols were tested. Here, these protocols will be referred to as 1.5% ISO, 1.0% ISO and MED + ISO. The 1.5% ISO and 1.0% ISO protocols were different only in the percentage of isoflurane (1.5% and 1.0%) used to maintain different depth of anesthesia. In the MED + ISO protocol we injected 0.05 mg/kg body weight of medetomidine intraperitoneally 5 min prior to inducing anesthesia and the isoflurane level was set at 0.75%. In all three protocols anesthesia was induced with 5% isoflurane for exactly 70 s, followed by 140 s of 1.5% ISO and finally the reduced level according to the respective protocol for at least 4 min for maintenance of steady-state before start of data acquisition. Isoflurane was vaporized in 30% O2 and 70% N2O. Each mouse (n = 9) was imaged at least three times per condition in a randomized manner.

To define functional networks (network study) and to assess changes in post-stroke functional connectivity (stroke study) only the MED + ISO protocol was used.

2.5. Imaging setup

In vivo widefield calcium imaging was performed with anesthetized animals being placed in a stereotactic frame below a customized imaging setup (Fig. 1a): A light beam of blue light emitting diodes (LED) of 445 nm nominal wavelength with 23 nm bandwidth (SOLIS 445B/M, Thorlabs, USA) and constant 650 mA current (Advanced Solis LED Driver, Thorlabs, USA) was redirected by a 495 nm dichroic longpass filter (Optical Imaging Ltd, Israel) into the optical path in front of the camera and through the chronic window on top of the skull into the cortex. The emitted light from the cortical GCaMP6s proteins passed through a set of two video lenses (NIKKOR, 85 mm f1.4, and NIKKOR 50 mm f1.2; Nikon, Japan) and a 495 nm dichroic longpass filter and a 515 nm longpass filter (both Optical Imaging Ltd, Israel). Working distance between the mouse cortex and first video lense was approximately 4.4 cm. The projected image was recorded by a 2/3″ Interline CCD camera with 7.4×7.4 µm pixel size (Adimec 1000-m/D, Adimec, Netherlands) and using a customized longDaq software (Optical Imaging Ltd, Israel) (Fig. 1b). The camera field-of-view covered a quadratic area of approximately 12×12 mm $= 144$ mm^2. Data was spatially binned at 3×3 pixels, resulting in an image matrix of 330×330 pixels (Fig. 1c).

2.6. Resting-state paradigm

Animals were anesthetized and fixed in a stereotactic frame to eliminate head motion. During the entire procedure the eyes were shielded from light. Images were recorded at a frame rate of 25 Hz. During the anesthesia study we recorded 200 s, resulting in 5000 frames per acquisition, in both other studies we recorded 240 s (=6000 frames) per acquisition (Fig. 1b). Acquisition duration was established at 240 s after it was determined via preliminary experiments that longer acquisition times did not provide any additional relevant advantages (Suppl. Fig. 2). In a subset of mice (n = 6) heart rate and respiratory rate was acquired simultaneously with calcium images, using the PowerLab data acquisition system (PowerLab 16/35, ADInstruments, New Zealand) and LabChart (LabChart, ADInstruments, New Zealand) (Fig. 1d–f).

2.7. Preprocessing of imaging data

All data processing steps were performed in MATLAB (R2016b, The MathWorks, USA). Aims of our preprocessing steps were to reduce noise and signal fluctuations such as signal decay due to GFP bleaching by the light beam during acquisition and signal fluctuations induced by heart and respiration rate. Calcium images were first resized by the factor of 2/3, using the MATLAB function imresize, resulting in an image matrix of 220×220 pixels and resolution of 18.5 pixel/mm. Then resting-state data was intensity normalized. This was done using the mean fluorescence intensity of the signal time course (F) as reference intensity to compute fluorescence signal difference of every time point (ΔF) which was subsequently normalized ($\Delta F/F$). Second, we applied a bandpass-filter with a passband from 0.1 to 1 Hz. This filter was implemented using the MATLAB functions cheby1 and filtfilt to design a Chebyshev Type I filter of order 2 and to perform zero-phase digital filtering. In a test data set heart and respiratory rate were always between the upper cutoff frequency of our filter (1 Hz) and the Nyquist frequency of 12.5 Hz, allowing their alias free removal by the bandpass filter (Fig. 1d–f). The lower bound of the filter was used to remove low frequency components such as the signal decay due to GFP bleaching. In preliminary experiments, we found GCaMP signal dominating the data, so no further preprocessing (e.g. to account for hemodynamic absorption) was performed (Suppl. Fig. 3). Filtered signal time courses were then cropped 10 s from beginning and end to reduce possibly remaining filter artifacts. An exemplary raw signal and corresponding preprocessed signal time course is shown in Fig. 1g. After preprocessing, videos were generated (Suppl. Video 1) to evaluate the recording and preprocessing quality. An experienced rater reviewed the video of each recording for motion artifacts and excluded affected acquisitions as soon as one single movement of the mouse was visually detected. This resulted in 27 (out of 30, 10% excluded) acquisitions for 1.5% ISO, 30 (out of 41, 26,8% excluded) acquisitions for 1.0% ISO and 25 (out of 34, 26,5% excluded) acquisitions for MED + ISO protocol during anesthesia study. In the stroke study, the final number of acquisitions was 256 (out of 279, 8.2% excluded).

2.8. Spatial registration

Preprocessed images from different days and animals were spatially registered to ensure intra- and interindividual correspondence of the analyzed cortical regions. To this end, all images were repositioned with their bregma in the center of the image matrix and the sagittal suture in a vertical line. This was achieved in one step for the first acquisition of every individual mouse by manually rotating and translating it in the image plane into a virtual space (3 degrees of freedom). For all following acquisitions of the same individual mouse, two steps were needed. In a first step images were manually aligned to the first (non-repositioned) acquisition by means of vasculature and anatomical landmarks. The hereby estimated transformation matrix was then combined in a second step with the transformation matrix associated with the spatial repositioning of the first acquisition, in order to reposition all acquisitions in the same way and—importantly—with only a single interpolation step (Fig. 1h).

2.9. Masking of images

An individual mask was created for every acquisition in a two-step process. First, a general mask was used to limit the analysis to cortical areas in the focal plane and exclude more laterally located cortical areas, which were out of focus due to the curvature of the cortical surface. The masking area was chosen by comparing the registered images from different animals and covered a symmetric area in both hemispheres (Fig. 1i). Secondly, an individual mask was computed which excluded all pixels saturated due to autofluorescence, e.g. in areas affected by the infarct. For every acquisition the two masks—general mask and individual mask—were combined. These resulting masks were used for all following analyses to identify included pixels and their signal time courses. The saturated pixels were used for lesion size estimation and depiction.

2.10. Power spectrum calculation

The periodogram function in MATLAB was utilized to calculate power spectral densities (or simply power spectrum). In order to construct spectrograms, the power spectral density was computed within a moving time window of 250 frames (=10sec), moving frame-by-frame over the entire signal time series. Spectrograms were calculated for the raw signal time courses of 6 arbitrarily preselected pixels which were located for all individuals consistently in the same cortical locations, due to spatial registration and subsequently averaged across these 6 pixels. An exemplary spectrogram and heart and respiratory rate for the same acquisition are depicted in Fig. 1e.

In the anesthesia study, the power spectrum was calculated for the preprocessed signal of three randomly but consistent preselected pixels in the right hemisphere and then spectral edge frequencies (SEF) and median frequency (MF) were derived as the frequencies at which the cumulative power reached respectively 5% (SEF 5), 50% (MF) and 95% (SEF 95) of the total power. A paired T test with subsequent Bonferroni correction was used for statistical testing of group differences.

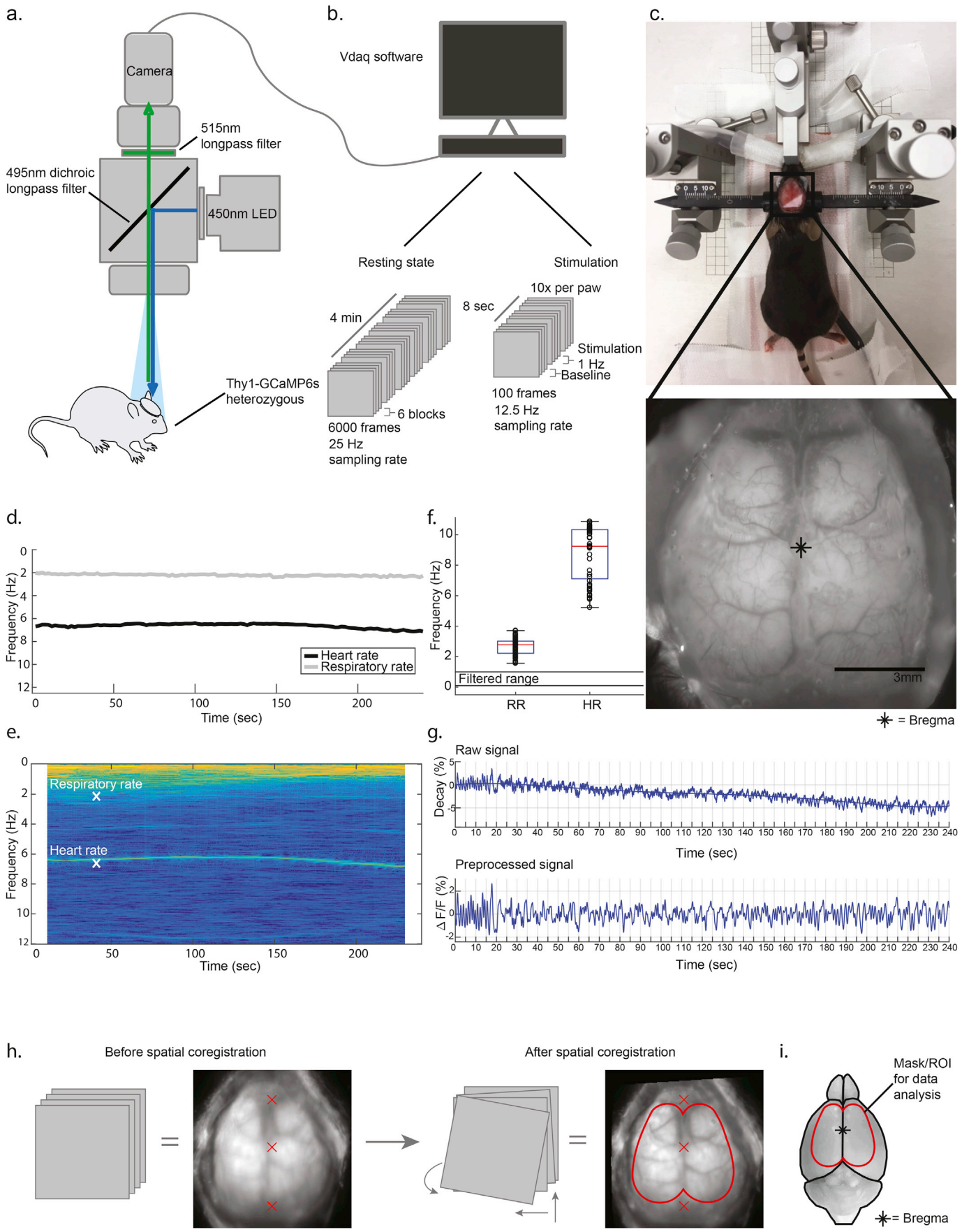

(caption on next page)

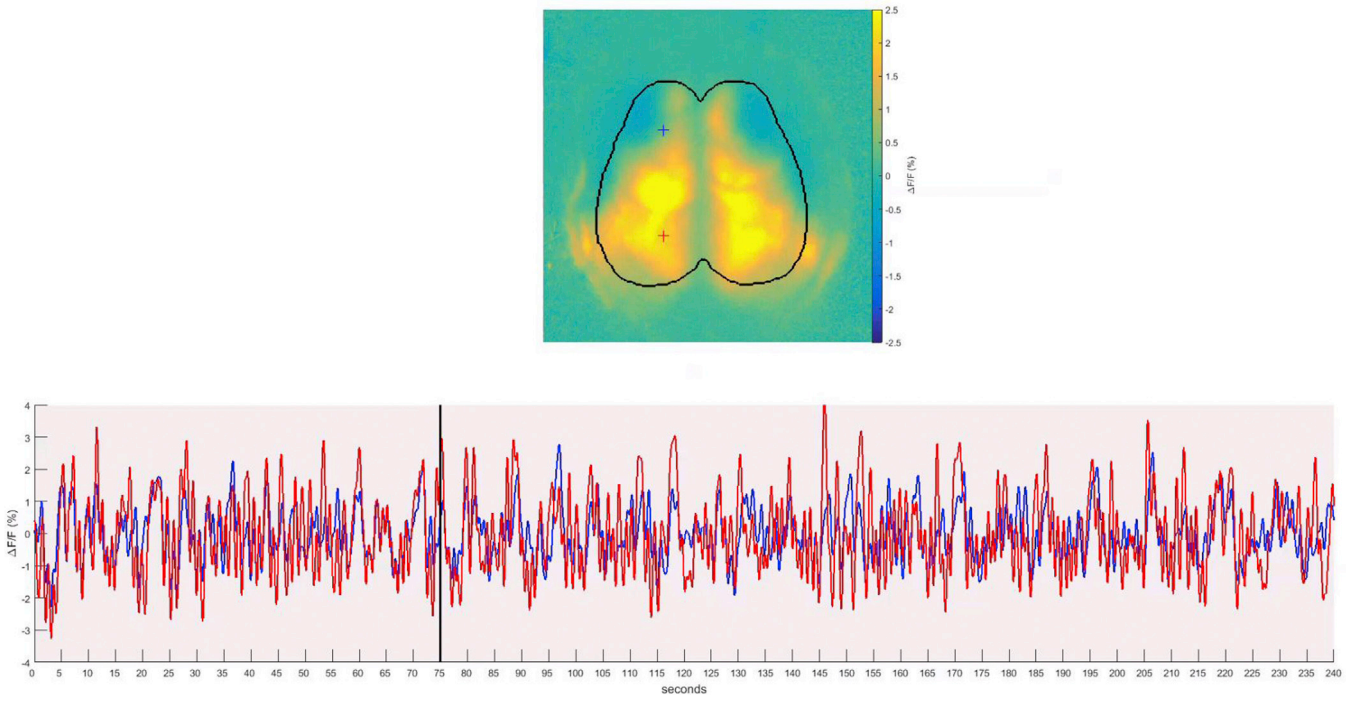

Multimedia component 3. figs13

2.11. Approximate entropy estimation

In order to select an optimal anesthesia protocol in the anesthesia study and to ensure moderate levels of anesthesia with comparable neuronal activity throughout experiments, approximate entropy (ApEn) was estimated. ApEn was computed for the preprocessed signal time series of three pixels located in the right hemisphere, using the MATLAB file exchange function calculating fast approximate entropy, offered by Kijoon Lee (2012). We decided to use the commonly used embedding dimension m = 2 (Chon et al., 2009). ApEn was then calculated for a range of tolerance levels (tolerance = r*std, with the coefficient r being varied between 0.01 and 0.3 by steps of 0.01, and std being the standard deviation of the signal time series). The resulting ApEn scores were averaged across the three pixels, but separately for each tolerance level. Then the maximum approximate entropy ($ApEn_{max}$) was determined among all tolerance levels to obtain an appropriate value for every data set as discussed by Chon et al. (2009). Paired T tests and subsequent Bonferroni correction was used for statistical testing of group differences in the different anesthesia protocols.

Based on comparisons between the different anesthesia protocols in the pilot experiment, we defined a threshold for $ApEn_{max}$ equal to 1.25 and excluded all recordings from the stroke study with $ApEn_{max}$ below this threshold (4 out of 279 acquisitions = 1.4% of the recordings).

2.12. Independent vector analysis

Independent vector analysis (IVA) as implemented in the Group ICA Of fMRI Toolbox (GIFT v3.0a; http://mialab.mrn.org/software/gift) was used to derive functionally independent cortical networks. IVA is an extension of ICA enabling its application to group data (Hutchison and Mitchell, 2010; Lee et al., 2007, 2008) and was recently suggested as an alternative to the widely used group independent component analysis (GICA), as it could be shown to better preserve subject variability (Michael et al., 2014). We used the algorithm to conduct both single subject analysis and cross-sectional group analysis in naïve mice. The number of components to be estimated by the algorithm has to be pre-selected. We used 20 components for single subject analysis and repeated the group analysis with increasing numbers of components (i.e. 16, 18, 20 and 30).

Single subject IVA was calculated for baseline data to locate the motor cortex for every mouse individually. The motor cortical region of the forepaw was identified by selecting the component, whose spatial map included a functional area located rostrolateral to the bregma. The coordinates of the peak pixel—the pixel with the highest correlation of its signal time course to the signal time course of the component—of this area were further used for motor cortex stroke induction by photothrombosis.

Fig. 1. Imaging setup, data acquisition and processing steps. **a.** Customized imaging setup built with 450 nm LED light source which was directed via 495 nm dichroic longpass filter to illuminate the mouse cortex; emitted GFP light was filtered by a 515 nm longpass filter before being acquired by a CCD camera. **b.** Resting-state data was recorded in 6 blocks à 1000 frames with 25 Hz frame rate; stimulation data was obtained in 10 blocks à 100 frames with 12.5 Hz frame rate. **c.** Topview of a prepared mouse ready for imaging and display of one image frame. **d**. Exemplary vital parameters (heart rate (HR), respiratory rate (RR)) during data acquisition of one animal. **e.** Spectrogram of unfiltered raw signal of the same acquisition as in d. Mean HR and RR over time are indicated by white crosses. **f.** Mean HR and RR during resting-state imaging in Hz; range of frequencies kept after filtering is indicated by black lines (n = 6; >2recordings each). **g.** Exemplary signal time course of one pixel before and after preprocessing; to capture the low frequency drift, also the polynomial trend (order = 5, not used for preprocessing) is shown. Preprocessing included normalization and bandpass filtering from 0.1 to 1.0 Hz. **h.** Spatial registration process. Grey rectangles represent different data acquisitions of one mouse; An average across 8 acquisitions of one mouse is shown next to the schematic drawing, resulting in a blurred image due to misalignment. The first acquisition was repositioned with the bregma in the center and midsagittal line vertically oriented. Subsequent acquisitions of the same animal were aligned to the first acquisition by means of anatomical structures. The red line delineates the general mask. Red crosses depict references in virtual space. **i.** Schematic drawing of entire mouse brain, indicating position of bregma and general mask.

2.13. Definition of functional networks and ROI using IVA

In order to find functional cortical areas across all mice, a meta-analysis of several group IVA analyses was conducted. To get the most robust results 16 group IVAs were calculated. In particular, we analyzed data from two different large groups of naïve animals (n = 41 and n = 47), and each animal was recorded on two independent days over 4 min (=6000 frames). Hence, we received four datasets by keeping the first and second recoding separate. For each of these four datasets, we conducted four different group IVA by altering the number of requested components (n = 16, 18, 20, 30). We selected 10 out of these 16 analyses based on the criterion that IVA components should be consistently spatially represented across all group IVAs. In a second step, only individual components which were represented in at least 9 out of the 10 analyses were considered as robust, while less prevalent components were discarded for further analyses. The areas of the selected components were merged and the median of their peak pixel obtained. We used the median peak pixel in the sensorimotor cortex of both hemispheres to define circular regions of interest (ROI) centered on them, with a diameter of 8 pixels (≈0.43 mm) and containing a total of 49 pixels. These ROI were then used in further functional connectivity analyses. Also, these ROI were masked, as described above. A ROI was only included in an analysis if more than 75% of its pixel were located within the mask. The ROI signal time courses were calculated as the average signal time course of all pixels within the corresponding ROI.

2.14. Functional connectivity analysis

In order to evaluate the effect of anesthesia on functional connectivity in the anesthesia study and to characterize network changes in the brain after stroke in the stroke study, we conducted three types of connectivity analysis: seed-based analysis, ROI pair-wise analysis, and global connectivity analysis (only used in the stroke study).

For all three types of analysis, functional connectivity was computed as Pearson's correlation coefficients between signal time series of different ROI (as resulting from the IVA meta-analysis) or single pixels. Correlation coefficients were further Fisher z-transformed, in order to allow parametric statistical testing and more accurate evaluation of high connectivity levels.

For seed-based functional connectivity analysis, connectivity scores were calculated between a selected ROI in the right caudal forelimb (rCFL; here considered the seed of analysis) and the signal time series of respectively all pixels on the cortical surface included within the mask. This analysis resulted in a map of connectivity scores. For ROI pair-wise analysis, connectivities were calculated between selected pairs of ROI and represented both as graph plots and as matrices. In graph plots, connections were represented as lines between ROI center-coordinates displayed topographically on top of an exemplary masked mouse cortex.

In the anesthesia study, connectivity scores were averaged across trials within condition, but separately for each individual mouse. Paired T tests and Bonferroni correction were used to compare these average scores between conditions. For visualization, these scores were further averaged across mice within each anesthesia condition. In the stroke study, two sample T test and Bonferroni correction was used for statistical comparison between stroke and sham groups at each time-point. If a ROI was located within or at the edge of a cortical area affected by autofluorescence, the connectivity scores calculated for this ROI were excluded from the analysis. If this masking procedure caused the sample size to drop for a specific ROI-pair or ROI-pixel-pair below 5 mice per group (i.e. stroke or sham group), this pair was excluded from analysis. For visualization, connectivity scores were averaged across mice within each treatment group.

Size of the contralesional motor cortex was assessed after calculation of seed-based functional connectivity in the rCFL. Quantification of the size of the rCFL area was done by calculating the sum of pixels with functional connectivity >2.25 in the same hemisphere only. Results were consequently normalized to baseline. Two sample T test and Bonferroni's correction was used for statistical analysis.

Global connectivity analysis (Cole et al., 2010; Rubinov and Sporns, 2011) was used to investigate overall functional connectivity alterations caused by the ischemic infarct in the stroke study. Global connectivity was computed for each pixel inside the contralateral hemisphere, as the average functional connectivity of this pixel with all other pixels inside the same cortical area. For statistical analysis of global connectivity alteration after infarct, baseline global connectivity scores were subtracted from the global connectivity scores at the days after stroke or sham procedure, for each mouse individually. For visualization, these differences in global connectivity were averaged within group and displayed in form of a topographical map for each time point. Instead, for statistical analysis these scores were further averaged across pixels, in order to receive one score per mouse and time point and compared at each time point between groups using two-sided T tests with Bonferroni correction. To further explore global connectivity alterations, the histogram of the distribution of non-normalized global connectivity scores across pixels was obtained at Baseline, D1 and D28 after stroke. For this purpose, global connectivity scores were averaged across mice per time point and pixel, for the stroke and the sham group respectively.

2.15. Stimulus dependent paradigm

Stimulation was performed subsequent to resting-state data acquisition at 12.5 Hz frame rate in a group of naïve animals (n = 23). Acupuncture needles (Hwato, Ternimed, Germany) were placed subcutaneously between second and third digit of each paw. Stimulus trigger was given by the Vdaq software (Optical Imaging Ltd, Israel), passed on to a Train/Delay Generator (DG2A, Digitimer Ltd, UK). The final stimulus was generated by a constant current isolated stimulator (DS3, Digitimer Ltd, UK). The stimulation protocol was determined in preliminary experiments according to two premises. First, we wanted to acquire pure sensory but no pain response. In order to fulfill this, we reduced mainly the frequency and number of applied stimuli. Secondly, we needed to obtain stable response in terms of successfully obtaining a cortical reaction to the stimulus as often as possible. This resulted in the following stimulation protocol: Paws were stimulated alternating and each paw was stimulated for at least two imaging blocks. Each block contained of 10 independent trials. Every trial lasted 8 s and started with a 2 s baseline period followed by 4 s of stimulation with maximum 1.6 mA amplitude, 300 ms duration and 1 Hz interval, and concluded with 2 s of resting period (Fig. 3 c).

2.16. Stimulation evoked activity

Signal time series recorded during paw stimulation were first normalized by subtracting and dividing through the average activity during the 2 s baseline period at trial start. The normalized time series were then averaged across trials, per each individual mouse and stimulated paw. In pilot studies, a stimulation-to-peak response delay measured approximately 380 ms. Therefore, frames recorded within a time window of 300–460 ms after stimulus onset (peak of response) and frames recorded within a time window 780–940 ms after stimulus onset (trough of response) were averaged, and then the peak to trough amplitude calculated as the difference between these averages. The peak to trough amplitudes for stimulations at different days were averaged per condition and mouse. Subsequently the interindividual mean per condition was calculated. Then, all pixels with a mean peak to trough amplitude above the 98th percentile were determined and considered as the somatosensory core region representing the stimulated paw area in the somatosensory cortex.

2.17. Photothrombosis

Photothrombosis was used to induce cortical focal ischemia. We

performed a baseline *in vivo* calcium imaging resting-state acquisition at least one day prior to stroke induction and calculated a single-subject IVA to obtain the motor cortex coordinates for each individual mouse. Animals received 10 µl/g body weight of 1% Rose Bengal dye in saline intraperitoneally (i.p.) 5 min prior to anesthesia (isoflurane in 30%O2/70%N2O). The mouse was then placed into a stereotactic frame. A laser (Cobolt HS-03, Solna, Sweden) with a fiber optic bundle of 1.5 mm diameter at the tip was used to induce a lesion restricted to the area of interest and the rest of the cortex was shielded from laser light. The infarct was induced through the coverslip, dental cement and intact skull by illuminating for 17 min at constant 561 nm wavelength and 25 mW output power at the fiber. Sham procedure was performed analogous, but without laser illumination.

Twenty-four hours after stroke induction, infarct area was measured via laser speckle contrast imaging using the PeriCam PSI System (PeriCam PSI System, Perimed, Sweden). Blood perfusion of the cortex was measured during 30 s and an averaged color coded picture obtained. The area with no and strongly reduced cortical blood perfusion was determined manually using ImageJ software (Version 1.49c, Fiji) (Schindelin et al., 2015).

2.18. Neuroscore

The neuroscore was assessed as previously published (Orsini et al., 2012). Briefly, the score is composed of the assessment of several subtests of both global and focal deficits. Assessment of global deficits included grooming, status of ears and eyes, posture, spontaneous activity and epileptic behavior. Focal deficits were evaluated by gait, grip, forelimb-asymmetry during tail suspension, circling behavior of both entire body or only forelimb, body symmetry and whisker response. Total score ranges from 0 to 54 points (26 point for general and 28 for focal deficits), higher score indicating worse deficits. Data was acquired once before stroke and on day 1, 3, 7, 14, 21 and 28 after photothrombosis. We used repeated measure 2-way-ANOVA and Sidak's correction for multiple comparisons for statistical testing.

2.19. Beamwalk test

The beamwalk test was performed by modifications as previously described (Luong et al., 2011). We used a 5 × 20 mm wooden beam. After training the mice at least 3 three days until successfully traversing the beam, a baseline run was recorded, after stroke data was acquired for day 3, 7, 14, 21 and 28 after stroke. On each testing day, every mouse had to run three times with a 30 s break in between. All trials were video recorded and analyzed frame by frame. Foot faults of the hindlimbs were counted for each paw separately and averaged for all three runs per time point. We used 2-way-ANOVA and Dunnett's correction for multiple comparisons for statistical testing.

2.20. Statistical analysis

Statistics for behavior analysis have been calculated using Graph Pad Prism. Statistics for *in vivo* calcium imaging experiments have been calculated in MATLAB. The applied statistical test is specified in the respective Methods section.

2.21. Data and Code

Data and Code will be made available on reasonable request to the corresponding authors.

3. Results

The overall aim of this study was to establish a translational procedure adopting analysis paradigms common in fMRI connectivity studies to a GECI-based neuronal activity imaging approach in mice. To achieve this, we performed a stepwise study design in three sub-studies, first analyzing a stringent mouse sedation protocol, then establishing network analyses in an experimental stroke model. The anesthesia study aimed to establish a sedation protocol allowing for stable and reproducible recordings of resting-state neuronal activity and to derive physiologically meaningful functional connectivity scores. The network study aimed to define functional cortical networks and to identify nodes in these networks which can be used as ROI for functional connectivity analysis in mice. The stroke study aimed to assess functional connectivity alterations after experimental stroke using the paradigm developed in the anesthesia and network studies.

3.1. Anesthesia study: determining the impact of anesthesia on functional connectivity analysis

We tested 3 protocols (n = 9; ≥3 acquisitions per protocol) differing in the depth of anesthesia: deep anesthesia with 1.5% isoflurane inhalation (1.5% ISO), low anesthesia at 1.0% isoflurane inhalation (1.0% ISO) and light sedation with a combination of medetomidine injection and 0.75% isoflurane inhalation (MED + ISO). The impact of anesthesia was already apparent in the preprocessed signal time courses and computed power spectra for the three anesthesia conditions (Fig. 2a and b). Moreover, both the spectral edge frequency (95th percentile, SEF95) and the maximum approximate entropy—a measure of randomness—differed significantly between all three anesthesia groups (Fig. 2c and d). The lowest entropy was observed in mice receiving the deeper anesthesia (1.5% ISO). We also investigated directly the impact of the different anesthesia protocols on functional connectivity. In a seed-based analysis, connectivity was calculated between a ROI of the sensorimotor cortex and the rest of the cortex (Fig. 2e). In this analysis considerable differences in functional connectivity were apparent. As the combination of ISO + MED preserved the largest degree of data entropy, largest spread in the frequency spectrum and was subjectively the most stable and reliable to handle protocol, this approach was used for the subsequent sub-studies: the “network study” and the “stroke study”.

3.2. Network study: identification of functional cortical networks by independent component analysis

Our primary aim was to map functionally relevant cortical areas in the mouse brain to obtain coordinates to use for further seed-based and ROI pair-wise connectivity analyses. To retrieve cortical networks, we performed a meta-analysis of 10 group-IVA which originated from different data sets and parameters (for more details see method section). This meta-analysis resulted in 12 components, with qualitatively similar spatial patterns in at least 9 out of the 10 IVAs (Fig. 3a, and Suppl. Fig. 4). For each of these 12 components, the corresponding spatial maps from the different IVAs were overlaid and pixels being in at least four analyses over-threshold in all these maps were marked as belonging to the cortical network described by that component (Fig. 3b, orange pixel). Furthermore, for each of these 12 components, the peak pixels in both hemispheres were determined in the spatial component maps from the different IVA and the median peak coordinates were subsequently calculated across the different IVA. The individual peak coordinates differed from the median peak coordinates on average by only 3.2 pixels (≈0.17 mm) (Suppl. Fig. 4i). The median peak coordinates were then used as center coordinates for ROI definition and interpreted as the center of the cortical areas involved in the functional networks captured by the IVA components (Fig. 3b). The function of these cortical areas was inferred by comparison of median peak coordinates to the Paxinos Brain Atlas (Franklin and Paxinos, 2007) (Suppl. Fig. 4 and Suppl. Table 1). We further aimed to validate the biological significance of identified components performing a somatosensory stimulation of all 4 paws (n = 23; Fig. 3c). We detected a specific response of the components identified as the sensory cortex (using the Paxinos atlas (Franklin and Paxinos, 2007)) to the stimulus, whereas the components identified as motor cortex did

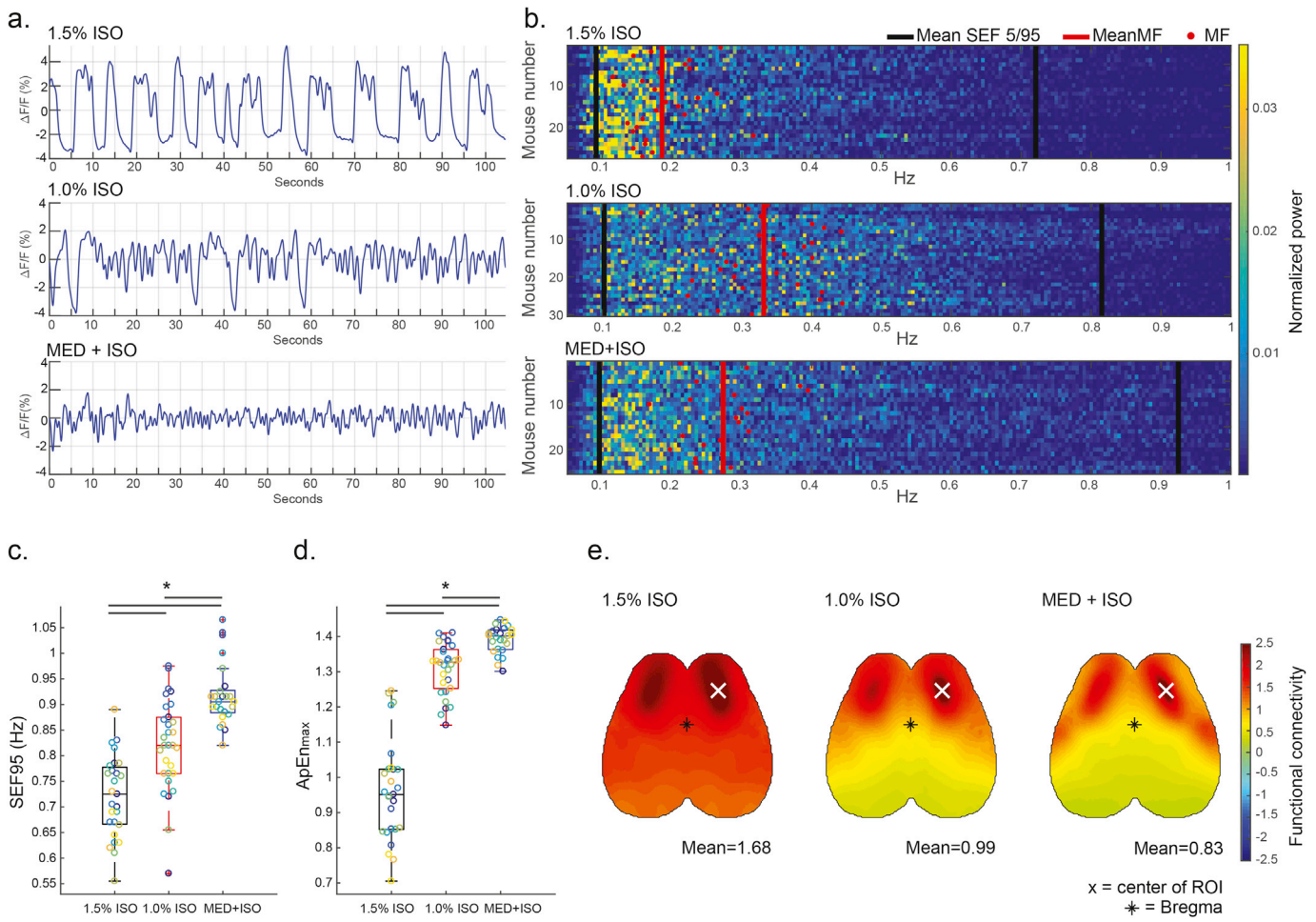

Fig. 2. Influence of anesthesia depth on calcium recordings and functional connectivity. a. Representative plots of filtered signal time course for all three anesthesia conditions. **b.** Power spectra for all trials in each anesthesia condition, normalized to the total power. Lines display median (red) and spectral edge frequencies (black) of the 5th (SEF 5) and 95th (SEF 95) percentile. **c.** Mean SEF 95 and **d.** mean maximum approximate entropy ($ApEn_{max}$) for each trial in the three anesthesia conditions. Each individual mouse is displayed in a different color. Significance bars above the plots indicate differences between conditions at a significance level $\alpha = 0.05$. **e.** Topographic depiction of seed-based functional connectivity averaged across mice; * = Bregma, white cross indicates seed.

not react to stimulation (Fig. 3d). Stimulation evoked contralateral activation of defined cortical areas, which were symmetrical when comparing left and right stimulation (Fig. 3e). An overlay of the components identified by IVA in the somatosensory cortex onto the areas of maximal activation in response to electrical paw stimulation (ΔF/F 98th percentile) revealed a high overlap (Fig. 3f). These findings indicate that the IVA analysis pipeline is able to perform unbiased identification of anatomically and functionally distinct cortical areas with neurophysiological function.

3.3. *Stroke study: assessment of functional connectivity after experimental stroke*

As a last step, we applied our novel approach to assess pathological changes and monitor recovery of functional connectivity after an acute injury to the motor cortex. We induced a photothrombotic lesion in the motor cortex (n = 23) which was identified by ICA of all individual animals. Control animals received sham surgery (n = 17). Two mice of the stroke group died during experiments (D7 and D35 post lesion). However, their acquired imaging data and behavior testing were included in the analysis. We then performed widefield calcium imaging as well as behavioral testing on days 1, 3, 7, 14, 21, 28 and 56 after surgery. First, we wanted to identify the infarcted area in our imaging data to exclude it due to potential imaging artifacts. We could show a high correlation ($R^2 = 0.704$; $p < 0.0001$; n = 23) of the area of saturated pixels and area of blood flow reduction assessed by laser speckle imaging on D1 after stroke (Suppl. Fig. 5). Hence, cortical autofluorescence of necrotic brain tissue was used to determine the lesion size and location as well as their temporal evolution until day 56 after stroke (Fig. 4a and b): After stroke we detected a massive increase of autofluorescent pixel in the stroke group, which decreased during recovery phase as a sign of longterm lesion involution. Consequently, pixels affected by cortical autofluorescence were excluded from further analyses in order to minimize potential bias by imaging artifacts. Additionally, we assessed bodyweight at baseline (Fig. 4c) and deficits in commonly used behavior tests for post-stroke motor deficits in the photothrombotic lesion model (Fig. 4d and e; Suppl. Table 2). Deficits in motor function were clearly detectable during the acute phase (days 1–7 after stroke) in the composite neuroscore as well as the beamwalk test. However, while the neuroscore still identified a significant behavioral deficit though with a recovery plateau from day 7 onwards up to 56 days, no significant deficits were detectable in the beamwalk test after 14 days post-lesion. Hence, behavior tests might be suitable to determine motor deficits in the acute phase after stroke. Whether incongruent findings in different tests are due to partial recovery, compensation or low sensitivity to analyze long-term recovery, is once more stressing the need for *in vivo* imaging application such as our tool to measure recovery by more sensitive and complementary means.

Analysis of functional connectivity was performed using the resting-state widefield calcium imaging paradigm, as established in the anesthesia and network sub-studies. Changes of functional connectivity

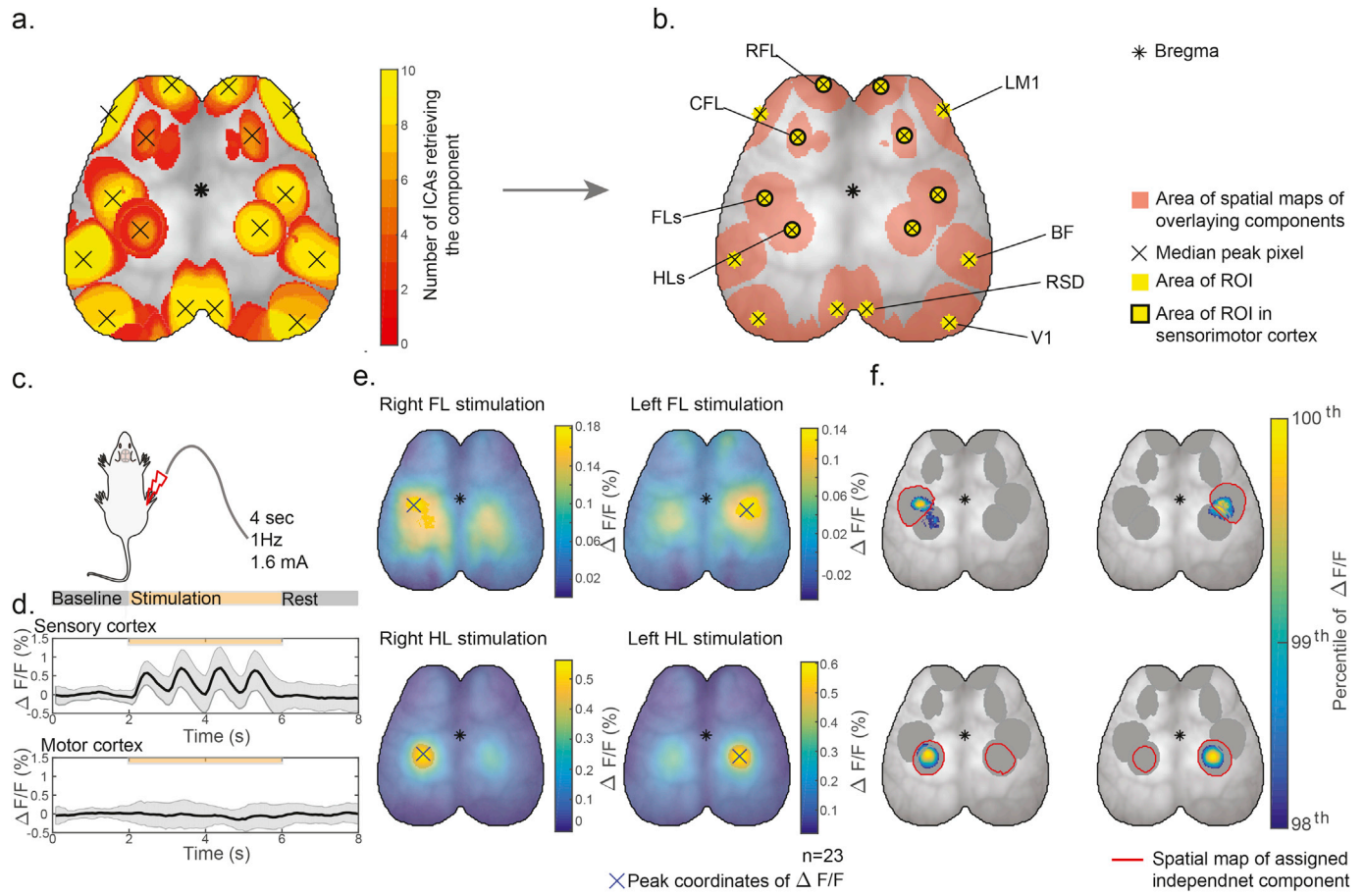

Fig. 3. IVA derived functional networks and validation by somatosensory stimulation. a. Topographical heatmap of the 12 components retrieved by the meta-analysis of 10 group IVA. Pixel-color indicates, in how many of the group-IVA a given pixel was present. **b.** Topographical depiction of all regions of interest (ROI) (yellow). The centers of the circular ROI (crosses) were determined as the median peak pixels of the matching IVA components. ROI were anatomically assigned as rostral forelimb area (RFL), lateral M1 motor cortex (LM1), caudal forelimb area (CFL), forelimb sensory (FLs), hindlimb sensory (HLs), barrel field (BF), retrosplenium (RSD) and primary visual cortex (V1). **c.** Experimental setup of paw stimulation paradigm; 10 trials were recorded successively, one trial consisted of 2 s baseline activity, followed by 4 s of 1 Hz stimulation (with stimuli of 1.6 mA and 300 ms duration) and 2 s resting period. **d.** For the example of hind limb stimulation in one animal, the evoked response (averaged across trials) in the contralateral sensory (ROI in HLs) and motor cortex (ROI in CFL) is shown at the bottom of the panel; black line corresponds to the mean, grey area to the range of standard deviation. **e.** Topographical depiction of mean ΔF/F of 23 mice for each stimulated paw (right and left forelimb (FL) and right and left hindlimb (HL)) **f.** Overlap of the 98th percentile of mean stimulation data (color coded), the areas retrieved by IVA analysis (grey) and assigned component (red). In b, c, f and g the star indicates the bregma as a spatial reference.

scores over time allowed us to track pathological changes and restoration of network integrity after photothrombotic motor cortex lesions. In line with previous findings (Bauer et al., 2014), we observed interhemispheric homotypic correlations as the dominant connectivity patterns in naïve brains (compare to Fig. 3 and BL images Fig. 5a–c). Therefore, we utilized the ROI corresponding to the structurally intact motor area contralateral to the lesion (the right caudal forelimb area; rCFL in Fig. 3b) as a seed to compute functional connectivity to all other pixels in the cortex (Fig. 5a). After infarction, we detected reduced interhemispheric connectivity of this rCFL ROI to the hemisphere ipsilateral to the infarct, in contrast to its rather unaffected intrahemispheric functional connectivity. The reduced interhemispheric connectivity persisted until 56 days post lesion. Additionally, to this seed-based connectivity analysis, we also conducted ROI pair-wise analysis using the 8 ROI (4 in each hemisphere), determined by the group-IVA in naïve animals and being located in the sensorimotor cortex (see Results, second section, and Fig. 3b). Corresponding to the seed-based connectivity analysis, also this pair-wise analysis of ROI in functionally defined cortical areas revealed a loss in connectivity to the ischemic area resulting in broad network disturbances after infarction (Fig. 5b–d). Interestingly, homotypic connectivity of the structurally unaffected motor cortex frontal to the lesion area (RFL = rostral forelimb motor cortex) was diminished until 28 days after stroke. In contrast, connectivity to the somatosensory cortex caudal to the infarcted cortex area remained mainly unaffected after stroke despite a similar distance to the lesion core (Fig. 5e and f), indicating more pronounced disturbances of connectivity in functionally linked networks such as the motor cortex. Interestingly, we observed a transient increase in contralateral connections which normalized to baseline levels already at day 3 after stroke (Fig. 5g). Consequently, a complex pattern of connectivity time courses can be observed after stroke with partial reconstitution of connectivity to some areas, unaffected connectivities to more remote network components as well as sustained reductions in connectivities to the primarily injured cortex area (i.e. lCFL) (Fig. 5e and f). Given the observed increase in contralateral functional connectivity, we additionally aimed to study more global consequences of acute injuries on cortical network function. We computed global connectivity to examine the overall functional connectivity of each pixel of the cortex relative to all other pixels (Cole et al., 2010; Rubinov and Sporns, 2011). In this analysis, we reduced the masked area to include only the hemisphere contralateral to the infarct in order to examine possible remote effects of the ischemic infarct in the non-lesioned hemisphere. We observed a significant transient increase in contralateral global connectivity at day 1 post injury. Especially regions in the sensory-motor system were affected by this transient change and returned to levels comparable

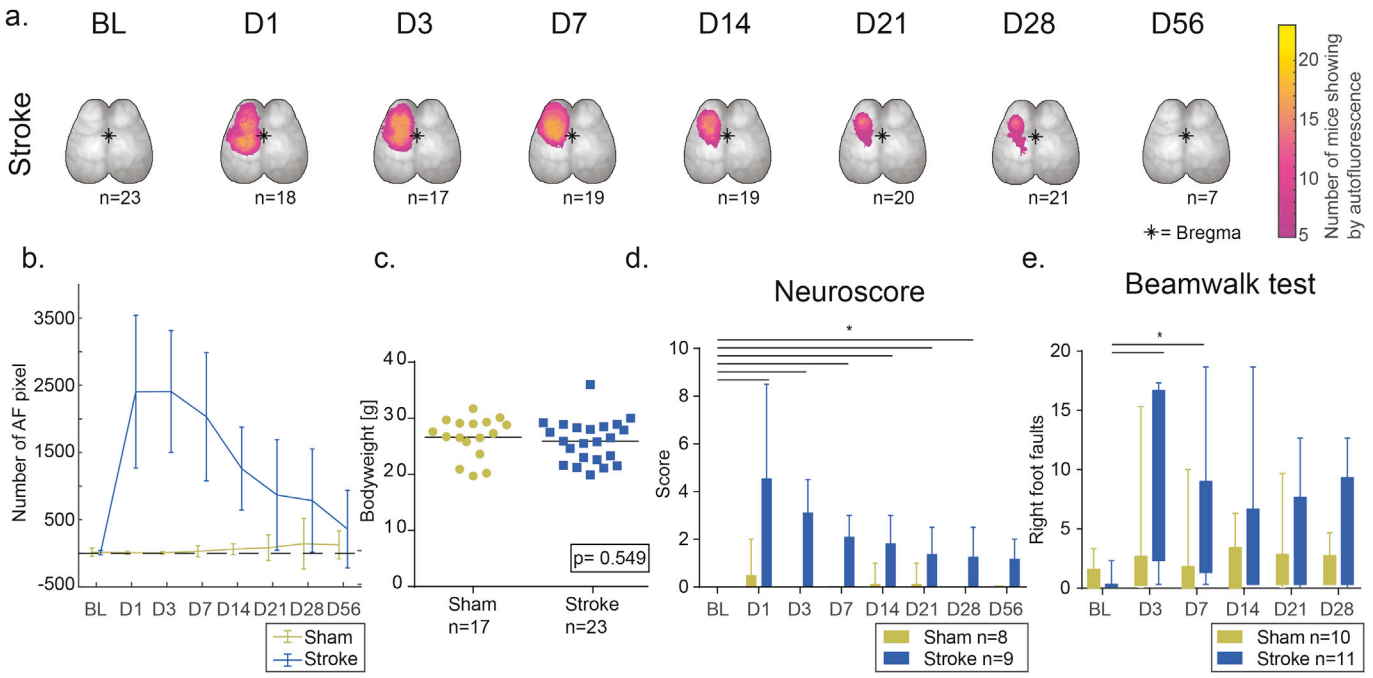

Fig. 4. Lesion incidence maps and behavioral deficit after stroke. a. Lesion distribution based on cortex autofluorescence after stroke for each acquisition time point. **b.** Quantification of autofluorescent pixel seen in widefield calcium imaging after stroke over time. **c.** Bodyweight of the two groups at baseline. **d.** Time course of the multi-parameter neuroscore (sham: n = 8, stroke: n = 9) and **e.** right foot faults counted during beamwalk test (sham: n = 10, stroke: n = 11). Statistical values have been calculated using repeated measure 2 way-ANOVA, * = $p < 0.05$; for more details see Suppl. Table 2.

with the sham-operated control group (Fig. 6a and Suppl. Fig. 6) In addition, we observed transient changes in the size of the contralateral motor cortex (Fig. 6b). This increase correlated with strong behavior deficits (Fig. 6c) and normalized during the recovery plateau.

4. Discussion

Taken together, our results demonstrate that our approach–the combination of controlled sedation, reproducible data acquisition and translational analysis protocol—is a robust and highly sensitive method to determine changes in cortical functional connectivity after stroke. The developed anesthesia protocol and analysis algorithms allow the analysis of complex changes in functional connectivity during the time course of post-stroke recovery and provide a meaningful complementation to the conventional method to determine recovery in experimental stroke research by behavior testing.

4.1. Widefield calcium imaging is a translational method

Investigation of brain function by electroencephalography (EEG) and fMRI plays a key role in translational neuroscience and clinical neurology. These methods have increased our knowledge on healthy and pathological brain function in patients. In order to successfully bridge preclinical models and clinical trials it is necessary to maximize the comparability of research approaches, interventions and diagnostic techniques. However, ensuring that a biological effect does not become „lost in translation“ relates not only to the way drugs are applied, animals are handled or data are reported. Comparability of the readouts is an equally critical measure that is currently still widely neglected (Bath et al., 2009; Dirnagl and Fisher, 2012; Howells et al., 2012). Comparable approaches to study function of the entire forebrain in laboratory mice are currently very limited. We combined and advanced the method of *in vivo* calcium imaging (Silasi et al., 2016; Vanni and Murphy, 2014) with commonly used algorithms from fMRI and EEG analysis to fill in this gap of translational methods for characterization of functional networks. Our tool provides better spatial and temporal resolution of brain activity than fMRI in mice, at the expense of acquiring only cortical information. Additionally, this imaging modality allows high reproducibility, low stress levels for the mice by having short procedure times, and low cost compared to fMRI. We offer three major enhancements: An advanced analysis approach in conjunction with establishing of a rigorous protocol of minimal sedation for reproducible imaging conditions and spatial alignment of different recordings of the same mouse as well as recordings from different mice. Due to these advances our novel tool represents a substantial improvement over previously developed, similar approaches for *in vivo* widefield neuronal calcium imaging (Kozberg et al., 2016; Ma et al., n.d.; Matsui et al., 2016; Silasi et al., 2016; Vanni and Murphy, 2014; Wright et al., 2017) which will allow a previously unprecedented comparability in the interpretation of functional neural networks between mice and men.

4.2. Comparability of widefield calcium imaging to other imaging modalities

In vivo widefield calcium imaging is still a new method in neuroscience. In the past, various other functional neuroimaging modalities have been established for rodent research such as two-photon imaging, intrinsic optical imaging, fMRI and positron-emission tomography (PET). Two photon imaging provides very high resolution imaging of cortical structures including neuronal calcium concentrations, but are limited to only small cortical areas with up to maximally a few hundred neurons and additionally requires invasive craniotomy and implantation of cranial windows. In contrast, our tool offers acquisition of whole forebrain neural activity at the expense of losing single neuron resolution. This holistic approach on network function by our widefield imaging procedure allows a more differentiated analysis of various functional domains of the cortical network in contrast to the widely used multiphoton imaging of small cortical areas. Additionally, our tool does not require trepanation of the skull and window implantation which might affect cortical function. Other often used imaging modalities such as positron-

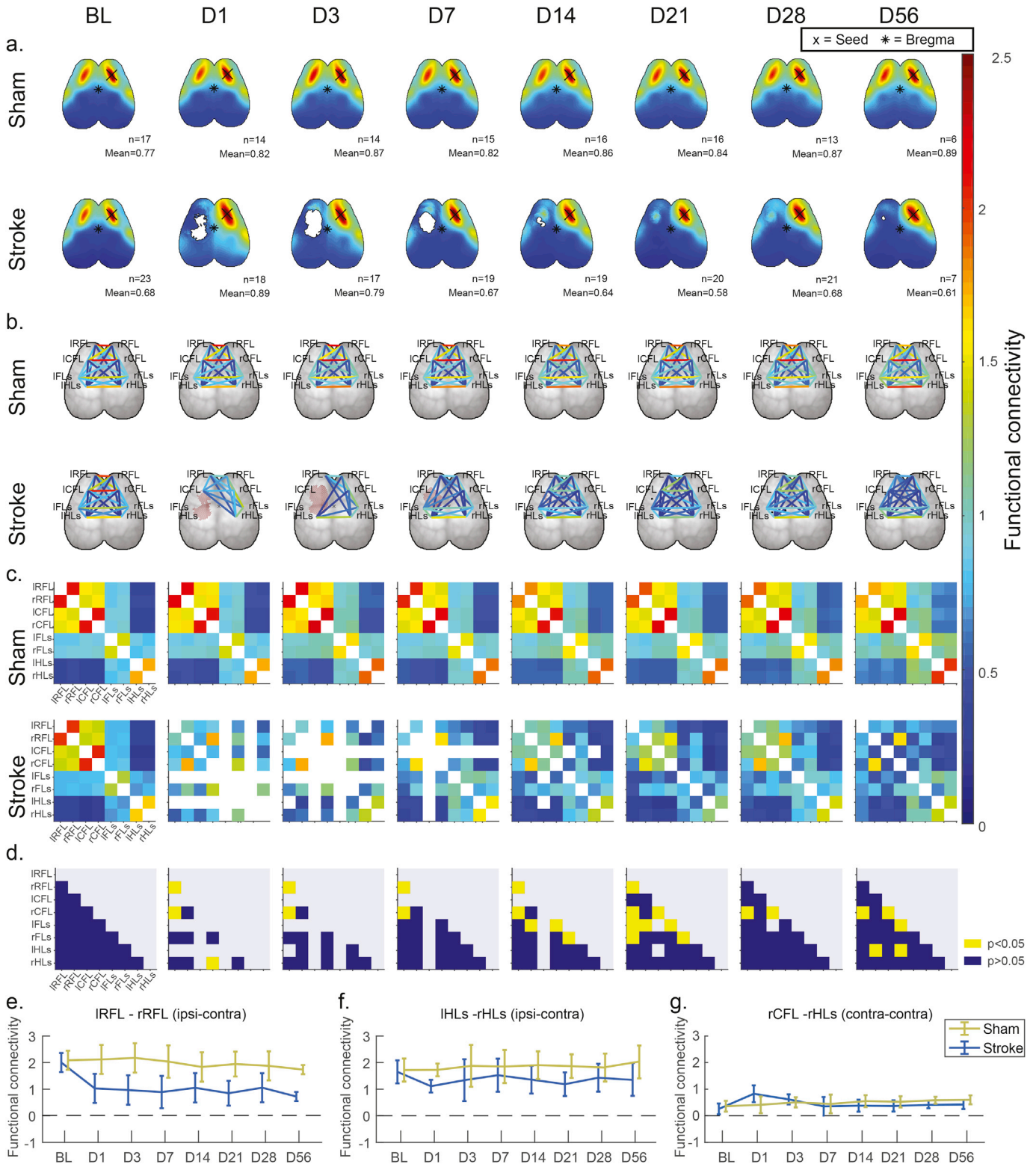

Fig. 5. Changes in functional connectivity after stroke. Each column in panels **a.** to **c.** depicts functional connectivity scores (averaged within sham and stroke group) for respectively one day (BL: baseline; D1-D56: days 1–56 after surgery). **a.** Topographical depiction of seed-based functional connectivity. The seed pixel (X) is located in the right caudal forelimb (rCFL) cortex, the area contralateral to the infarct. **b**. Graph-representation and **c.** matrix-representation of functional connectivity between 8 ROI, 4 in each hemisphere placed in rostral forelimb (RFL), caudal forelimb (CFL), hindlimb sensory (HLs) and forelimb sensory (FLs) areas, r and l refer to right or left hemisphere respectively. Functional connectivity is displayed as Fisher z-transformed Pearson's correlation; squares which contain less than 5 data points are not displayed. **d.** Results of T test between sham and stroke for each acquisition time point; p values were corrected via Bonferroni correction for multiple testing. Color codes indicate a significant group difference (p-corrected<0.05) in yellow. Functional connectivity between **e.** right and left CFL **f.** right and left HLs and **g**. right CFL and HLs in sham and stroke operated groups. Data points and error bars represent mean and standard deviation.

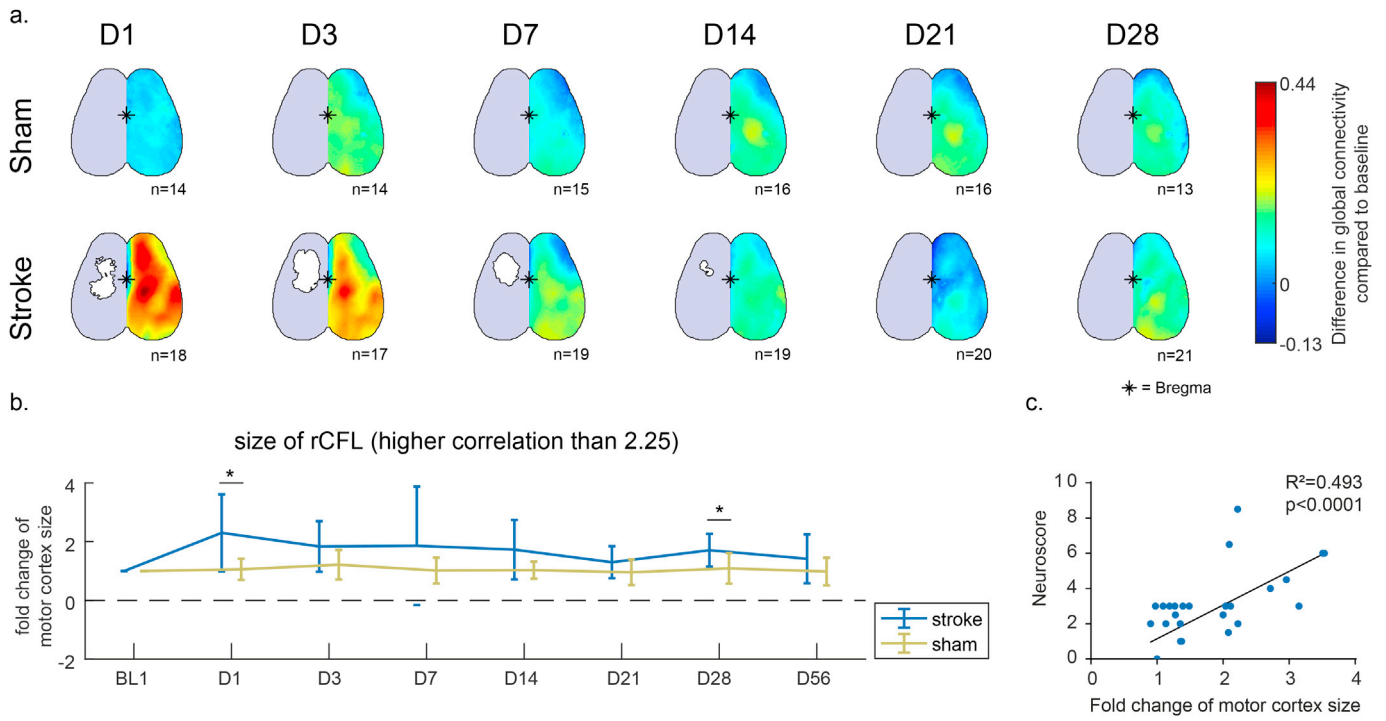

Fig. 6. Analysis of contralateral global connectivity after stroke. a. Depiction of the mean change in global connectivity after surgery (D1-D28: days 1–28 after surgery) at each pixel in the contralateral hemisphere. Change in global connectivity was calculated by subtracting for each pixel the baseline global connectivity at the same pixel. **b.** Quantification of contralateral motor size; all pixel with higher seed-based functional connectivity than 2.25 were taken into account; data is normalized to baseline; stars indicate significant group differences (p-corrected<0.05) **c.** Correlation between behavioral deficits measured by neuroscore and contralateral motor size.

emission tomography (PET) and fMRI are still very challenging in small rodents due to the complexity and costs of such a setup (Schroeter et al., 2014; Zerbi et al., 2015). Although these modalities provide the possibility of investigating the entire brain and not only cortical structures, they lack both high spatial and temporal resolution. Moreover, fMRI and PET usually require deeper anesthesia compared to our tool, which will affect neuronal function as clearly demonstrated in our study. Thereby, widefield calcium imaging expands existing options such as two-photon imaging to display larger structures up to the entire forebrain cortex and has the potential to become a routine technique for studying network function in mice (Kozberg et al., 2016; Ma et al., n.d.; Matsui et al., 2016; Silasi et al., 2016; Vanni and Murphy, 2014; Wright et al., 2017).

4.3. Neural activity and neurovascular coupling

In the healthy brain, localized neural activity and blood flow regulation are closely linked by a mechanism known as neurovascular coupling, which is a multicellular process encompassing neurons, glia and vascular cells (Iadecola, 2004; Lauritzern, 2005). However, brain disorders such as Alzheimer's disease and stroke impair physiological neurovascular coupling (Balbi et al., 2017; Iadecola, 2004). This impairment plays a pivotal role in blood-flow-dependent imaging modalities such as fMRI or intrinsic optical imaging, because the possibility to draw conclusions on neural activity is based on the assumption of an intact neurovascular coupling. In contrast, our tool allows the blood-flow independent measurement of neural activity by primarily directly measuring the signal (GCaMP fluorescence) from excitatory neurons. As an important limitation, our set-up cannot provide measurement of hemodynamic changes simultaneously to GCaMP recording. Previous studies have described that hemodynamic absorption can potentially interfere with GCaMP-derived neural signals, which would make simultaneous blood flow and calcium signal acquisition desirable as it would allow correction for such effects (Ma et al., 2016; Wright et al., 2017).

4.4. Reducing the effect of anesthesia on imaging data

An important consideration for the design of our imaging approach was to generate a widely applicable and relatively easy to use approach. Therefore, we chose to perform the imaging in anesthetized mice, even though awake-imaging is possible at expense of time investment to habituate the animals to experimental set-up (Silasi et al., 2016). Using anesthesia might of course limit the comparability to human data, however we aimed to reduce its interference. Anesthesia depth can affect neuronal activity, with deeper levels of anesthesia leading to slower activity with higher amplitude (Kiersey et al., 1951). This effect is likely to interfere with analysis of functional imaging data. During the process of finding an appropriate sedation protocol, we experienced imaging parameters to be very susceptible to the anesthesia depth. In contrast to some previous studies which reported comparable results in widefield calcium imaging between awake and anesthetized animals (Mohajerani et al., 2010; Silasi et al., 2016), our study revealed a profound impact of the anesthesia protocol on functional connectivity measures. We evaluated different parameters as surrogate markers for anesthetic depth. We identified the approximate entropy ($ApEn_{max}$) being highly influenced by the tested anesthesia protocols. This parameter has been previously reported to be affected by anesthesia also in EEG recordings during surgery (Bruhn et al., 2003, 2000; Liu et al., 2016) and was shown to equally perform as the commonly used bispectral index used in human surgery for control of anesthesia (Bruhn et al., 2006, 2003). Consequently, we used $ApEn_{max}$ as a measure for selection of the anesthesia procedure with the least impact on physiological randomness of the signal time series. Thereby, we identified light sedation to only minimally affect randomness as well as preserved a high spectral edge frequency the signal time courses which are well-established measures of depth of anesthesia (Bruhn et al., 2006; Drummond et al., 1991; Katoh et al., 1998). These are important findings with potential impact also on related imaging fields using anesthetized/sedated rodents, because the effect of anesthesia is

widely disputed and discrepantly reported in the literature. While some studies reported—consistent with our findings—a substantial influence of anesthesia on functional connectivity (Grandjean et al., 2014; Jonckers et al., 2014; Kalthoff et al., 2013; Nasrallah et al., 2014), others did not observe such an influence in their datasets (Mohajerani et al., 2010; Silasi et al., 2016). This discrepancy might be due to differences in imaging modality, analysis strategy but also the sensitivity to anesthesia-dependent effects in the different approaches. Yet, the effect was unequivocally evident in our standardized and randomized analysis and needs careful consideration in future studies. Therefore, we established a highly reproducible protocol for the standardized light sedation of animals with medetomidine and low-dose isoflurane and provide here a very detailed and easily reproducible protocol for this light sedation approach.

4.5. Functional ROIs for mapping the cortical connectome

ICA is a well-established method used with fMRI data to identify resting-state networks in the human brain (Calhoun et al., 2001; McKeown et al., 1998). To define functional networks we applied ICA to our resting-state dataset, more specifically a multivariate extension termed IVA. IVA was introduced by Lee et al. and is an alternate way of group fMRI analysis which avoids permutation ambiguity of ICA (Lee et al., 2007). Identification of networks via ICA is independent of a priori seed definition, region of interest or model time course (Michael et al., 2014). In human fMRI and EEG, it is well established that components retrieved by ICA are mostly overlapping with brain areas activated during tasks (Smith et al., 2009). To our knowledge we are first to validate this paradigm also in a rodent imaging approach by demonstrating overlap of cortical areas identified by ICA and somatosensory stimulation. Analogous to the experiments in humans, spatially overlapping results from stimulation and ICA analysis confirm the involvement of areas detected by ICA in particular sensory or motor functions. In comparison, existing imaging methods usually derive coordinates of ROI from sensory evoked responses or the stereotactic coordinates retrieved from brain atlases (Hakon et al., 2018; Mcgirr et al., 2017; Van Meer et al., 2010; Vanni et al., 2017; Vanni and Murphy, 2014). In contrast, ICA-derived coordinates provide functional ROI, where ROI determination and experimental investigation of associated parameters such as functional connectivity can be accomplished in the same *in vivo* experiment.

4.6. Quality management in analysis of functional imaging after stroke

As a proof-of-concept application of our tool in a disease model, we chose to investigate brain network changes after cortical ischemia in the motor cortex. Tissue necrosis induced by brain ischemia resulted in intensive autofluorescence of the lesioned cortical area. This was underlined by a linear correlation of the area of reduced blood-flow (Laser-speckle flowmetry) and the area of infarct-induced autofluorescence. A relevant concern for the image analysis was the possibility that the autofluorescence could affect the analysis signal variations in the adjacent cortical areas. In order to account for this technical limitation, we excluded all autofluorescent pixels from subsequent analyses. Furthermore, we used ROIs instead of single pixel reference points for the network analysis, as this will minimize potential interference of imaging artifacts particularly in the border zone of the ischemic area with single pixels. Unfortunately, this comes along with losing information of fine networks in the peri-lesional cortex, which might then be better assessed by different imaging modalities for small network analyses such as *in vivo* two-photon imaging of neuronal activity.

4.7. Changes in functional connectivity after stroke

Remote to the infarct we found changes in contralateral functional connectivity in post-stroke mice. Functional connectivity between contralateral motor and sensory cortex was increased and additionally, we found a temporary enhancement in contralateral global connectivity after lesion. This observation is in accordance with a previous study performed in rats using fMRI (Van Meer et al., 2010) and was also reported in human stroke patients (Bütefisch et al., 2008; Murase et al., 2004). Additionally, we detected a transient increase size of the contralateral motor cortex. In humans pathophysiological enhancement of activity of the contralateral motor cortex is well-described and associated with motor recovery (Grefkes et al., 2008; Grefkes and Fink, 2011; Rehme et al., 2011). Reduced interhemispheric disinhibition is speculated to play a role in this increased functional connectivity (Grefkes et al., 2008). Whether this increase in contralateral hemisphere activity is yielding positive or negative effects on recovery remains unexplored (Grefkes and Fink, 2011). We report normalization of all three parameters –global connectivity, increased contralateral intrahemispheric functional connectivity and size of the rCFL— being associated with the recovery plateau assessed by the neuroscore. This observation has also been reported in humans (Ward et al., 2003). Regarding interhemispheric connections, we found as previously reported very strong functional connectivity between homotypic areas of both brain hemispheres under healthy conditions (Bauer et al., 2014), which was significantly reduced after stroke in the acute and subacute phase. In our model the observed changes in functional connectivity remained localized to areas of the motor cortex but did not affect the somatosensory cortex. This post-stroke desynchronisation in neural activity might mirror changes due to both the acute injury and starting regenerative processes as well as secondary degeneration due to acute neuronal damage (Duering and Schmidt, 2017). Interestingly, a similar pattern of confined changes to closely associated cortex regions was previously also observed using stimulus-dependent imaging after cortical injuries (Lim et al., 2014) while subcortical lesions seem to have a more widespread impact also on distant functional systems such as both sensorimotor and visual system after subcortical stroke (Van Meer et al., 2010). At later time points we see improvement of interhemispheric functional connectivity which might be expression of restoration of bilateral brain communication and therefore a marker of regeneration. With regeneration of interhemispheric brain functional connectivity and normalization of contralateral motor cortex size, we see amelioration of behavioral deficits. Limitations of behavioral assessment.

Rodent behavior testing after acute brain injuries, however, has numerous limitations and is—although widely used in the research community—a rather insensitive and unspecific readout for neurological recovery (Balkaya et al., 2013; Llovera et al., 2015; Trueman et al., 2017). Besides the intrinsic limitations to assess complex neurological deficits by simplified tests in small rodents, also the interpretation of behavioral test results is largely rater-dependent and biased by the selection of the used tests. On the contrary, *in vivo* imaging of functional cortical networks provides unbiased, sensitive assessment of the recovery process. Moreover, our tool offers the possibility to analyze the nearly the entire forebrain cortex and hence different functional cortical systems simultaneously. Findings such as the involvement of different cortical functional systems, their degree of impact on regenerative processes or possible transient compensatory mechanisms, can then direct more in-depth analyses of the identified cortical systems of interest.

4.8. Conclusion

With *in vivo* widefield calcium imaging in combination with advanced analytical strategies such as ICA, we present an easy to handle method for repetitive study of functional cortical networks in mice. Particularly the comparability of analysis algorithms with human fMRI approaches will allow now urgently needed translational imaging studies from mouse to men for mechanistic studies and development of novel therapies.

Conflicts of interest

The authors declare no competing financial interests.

Acknowledgements

We thank Prof. Timothy Murphy (University of British Columbia, Vancouver, Canada) for constructive discussions on this tool. This work was supported by the Excellence cluster of the German research foundation "Munich Cluster for Systems Neurology (SyNergy)" and the German Research foundation [DFG, LI-2534/2-1 to A.L. & DU 1626/1-1 to M.D.]

Appendix A. Supplementary data

Supplementary data to this article can be found online at https://doi.org/10.1016/j.neuroimage.2019.06.014.

References

Balbi, M., Koide, M., Wellman, G.C., Plesnila, N., 2017. Inversion of neurovascular coupling after subarachnoid hemorrhage in vivo. J. Cereb. Blood Flow Metab. 37, 3625–3634. https://doi.org/10.1177/0271678X16686595.

Balkaya, M., Kröber, J.M., Rex, A., Endres, M., 2013. Assessing post-stroke behavior in mouse models of focal ischemia. J. Cereb. Blood Flow Metab. 33, 330–338. https://doi.org/10.1038/jcbfm.2012.185.

Bath, P.M.W., Macleod, M.R., Green, A.R., 2009. Emulating multicentre clinical stroke trials: a new paradigm for studying novel interventions in experimental models of stroke. Int. J. Stroke 4, 471–479. https://doi.org/10.1111/j.1747-4949.2009.00386.x.

Bauer, A.Q., Kraft, A.W., Wright, P.W., Snyder, A.Z., Lee, J.M., Culver, J.P., 2014. Optical imaging of disrupted functional connectivity following ischemic stroke in mice. Neuroimage 99, 388–401. https://doi.org/10.1016/j.neuroimage.2014.05.051.

Bruhn, J., Bouillon, T.W., Radulescu, L., Hoeft, A., Bertaccini, E., Shafer, S.L., 2003. Correlation of approximate entropy, bispectral index, and spectral edge frequency 95 (SEF95) with clinical signs of "anesthetic depth" during coadministration of propofol and remifentanil. Anesthesiol. J. Am. Soc. Anesthesiol. 98, 621–627.

Bruhn, J., Myles, P.S., Sneyd, R., Struys, M.M.R.F., 2006. Depth of anaesthesia monitoring: what's available, what's validated and what's next? Br. J. Anaesth. 97, 85–94. https://doi.org/10.1093/bja/ael120.

Bruhn, J., Rö, H., Hoeft, A., 2000. Approximate entropy as an electroencephalographic measure of anesthetic drug effect during desflurane anesthesia. Anesthesiology 92 (3), 715–726.

Bütefisch, C.M., Weßling, M., Netz, J., Seitz, R.J., Hömberg, V., 2008. Relationship between interhemispheric inhibition and motor cortex excitability in subacute stroke patients. Neurorehabilitation Neural Repair 22, 4–21. https://doi.org/10.1177/1545968307301769.

Calhoun, V.D., Adali, T., Pearlson, G.D., Pekar, J.J., 2001. Functional neuroanatomy of visuo-spatial working memory in turner syndrome. Hum. Brain Mapp. 14, 96–107. https://doi.org/10.1002/hbm.

Carter, A.R., Astafiev, S.V., Lang, C.E., Connor, L.T., Rengachary, J., Strube, M.J., Pope, D.L.W., Shulman, G.L., Corbetta, M., 2010. Resting inter-hemispheric fMRI connectivity predicts performance after stroke, 67, pp. 365–375. https://doi.org/10.1002/ana.21905.

Carter, A.R., Shulman, G.L., Corbetta, M., 2012. Why use a connectivity-based approach to study stroke and recovery of function? Neuroimage 62, 2271–2280. https://doi.org/10.1016/j.neuroimage.2012.02.070.

Chon, K., Scully, C., Lu, S., 2009. Approximate entropy for all signals. IEEE Eng. Med. Biol. Mag. 28, 18–23. https://doi.org/10.1109/MEMB.2009.934629.

Cole, M.W., Pathak, S., Schneider, W., 2010. Identifying the brain's most globally connected regions. Neuroimage 49, 3132–3148. https://doi.org/10.1016/J.NEUROIMAGE.2009.11.001.

Cramer, S.C., Nelles, G., Benson, R.R., Kaplan, J.D., Parker, R.A., Kwong, K.K., Kennedy, D.N., Finklestein, S.P., Rosen, B.R., 1997. A functional MRI study of subjects recovered from hemiparetic stroke. Stroke 28, 2518 LP-2527.

Dana, H., Chen, T.W., Hu, A., Shields, B.C., Guo, C., Looger, L.L., Kim, D.S., Svoboda, K., 2014. Thy1-GCaMP6 transgenic mice for neuronal population imaging in vivo. PLoS One 9, 1–9. https://doi.org/10.1371/journal.pone.0108697.

Dirnagl, U., Fisher, M., 2012. International, multicenter randomized preclinical trials in translational stroke research: it's time to act. J. Cereb. Blood Flow Metab. 32, 933–935. https://doi.org/10.1038/jcbfm.2012.51.

Drummond, J.C., Brann, C.A., Perkins, D.E., Wolfe, D.E., 1991. A comparison of median frequency, spectral edge frequency, a frequency band power ratio, total power, and dominance shift in the determination of depth of anesthesia. Acta Anaesthesiol. Scand. 35, 693–699. https://doi.org/10.1111/j.1399-6576.1991.tb03374.x.

Duering, M., Schmidt, R., 2017. Remote changes after ischaemic infarcts: a distant target for therapy? Brain 140, 1818–1820. https://doi.org/10.1093/brain/awx114.

Franklin, K.B.J., Paxinos, G., 2007. The Mouse Brain in Stereotactic Coordinates, third ed., third ed. Elsevier Inc.

Grandjean, J., Schroeter, A., Batata, I., Rudin, M., 2014. Optimization of anesthesia protocol for resting-state fMRI in mice based on differential effects of anesthetics on functional connectivity patterns. Neuroimage 102, 838–847. https://doi.org/10.1016/j.neuroimage.2014.08.043.

Grefkes, C., Fink, G.R., 2011. Reorganization of cerebral networks after stroke: new insights from neuroimaging with connectivity approaches. Brain 134, 1264–1276. https://doi.org/10.1093/brain/awr033.

Grefkes, C., Nowak, D.A., Eickhoff, S.B., Dafotakis, M., Küst, J., Karbe, H., Fink, G.R., 2008. Cortical connectivity after subcortical stroke assessed with functional magnetic resonance imaging. Ann. Neurol. 63, 236–246. https://doi.org/10.1002/ana.21228.

Hakon, J., Quattromani, M.J., Sjölund, C., Tomasevic, G., Carey, L., Lee, J.M., Ruscher, K., Wieloch, T., Bauer, A.Q., 2018. Multisensory stimulation improves functional recovery and resting-state functional connectivity in the mouse brain after stroke. NeuroImage Clin. 17, 717–730. https://doi.org/10.1016/j.nicl.2017.11.022.

Howells, D.W., Sena, E.S., O'Collins, V., Macleod, M.R., 2012. Improving the efficiency of the development of drugs for stroke. Int. J. Stroke 7, 371–377. https://doi.org/10.1111/j.1747-4949.2012.00805.x.

Hutchison, D., Mitchell, J.C., 2010. Latent Variable Analysis and Signal Separation, 9th Intern. Springer.

Iadecola, C., 2004. Neurovascular regulation in the normal brain and in Alzheimer's disease. Nat. Rev. Neurosci. 5, 347–360. https://doi.org/10.1038/nrn1387.

Jonckers, E., Palacios, R.D., Shah, D., Guglielmetti, C., Verhoye, M., Van Der Linden, A., 2014. Different anesthesia regimes modulate the functional connectivity outcome in mice. Magn. Reson. Med. 72, 1103–1112. https://doi.org/10.1002/mrm.24990.

Kalthoff, D., Po, C., Wiedermann, D., Hoehn, M., 2013. Reliability and spatial specificity of rat brain sensorimotor functional connectivity networks are superior under sedation compared with general anesthesia. NMR Biomed. 26, 638–650. https://doi.org/10.1002/nbm.2908.

Katoh, T., Suzuki, A., Ikeda, K., 1998. Electroencephalographic derivatives as a tool for predicting the depth of sedation and anesthesia induced by sevoflurane. Anesthesiology 88 (3), 642–650. https://doi.org/10.1097/00000542-199803000-00014.

Kiersey, D.K., Bickford, R.G., Faulconer, A., 1951. Electro-encephalographic patterns produced by thiopental sodium during surgical operations: description and classification. Br. J. Anaesth. 23, 141–152. https://doi.org/10.1093/bja/23.3.141.

Kozberg, M.G., Ma, Y., Shaik, M.A., Kim, S.H., Hillman, E.M.C., 2016. Rapid postnatal expansion of neural networks occurs in an environment of altered neurovascular and neurometabolic coupling. J. Neurosci. 36, 6704–6717. https://doi.org/10.1523/JNEUROSCI.2363-15.2016.

Lauritzern, M.J., 2005. Reading vascular changes in brain imaging: is dendritic calcium the key? J. Cereb. Blood Flow Metab. 25. S684–S684. https://doi.org/10.1038/sj.jcbfm.9591524.0684.

Lee, I., Kim, T., Lee, T.-W., 2007. Fast fixed-point independent vector analysis algorithms for convolutive blind source separation. Signal Process. 87, 1859–1871. https://doi.org/10.1016/J.SIGPRO.2007.01.010.

Lee, J.-H., Lee, T.-W., Jolesz, F.A., Yoo, S.-S., 2008. Independent vector analysis (IVA): multivariate approach for fMRI group study. Neuroimage 40, 86–109. https://doi.org/10.1016/J.NEUROIMAGE.2007.11.019.

Lee, K., 2012. Fast Approximate Entropy.

Lim, D.H., Ledue, J.M., Majid, X., Mohajerani, H., Murphy, T.H., 2014. Optogenetic mapping after stroke reveals network-wide scaling of functional connections and heterogeneous recovery of the peri-infarct. J. Neurosci. 43 (49), 16455–16466. https://doi.org/10.1523/JNEUROSCI.3384-14.2014.

Liu, Q., Chen, Y.-F., Fan, S.-Z., Abbod, M.F., Shieh, J.-S., 2016. A comparison of five different algorithms for EEG signal analysis in artifacts rejection for monitoring depth of anesthesia. Biomed. Signal Process. Control 25, 24–34. https://doi.org/10.1016/j.bspc.2015.10.010.

Llovera, G., Hofmann, K., Roth, S., Salas-Pérdomo, A., Ferrer-Ferrer, M., Perego, C., Zanier, E.R., Mamrak, U., Rex, A., De Simoni, M.-G., Dirnagl, U., Grittner, U., Planas, A.M., Plesnila, N., Vivien, D., Liesz, A., 2015. Results of a preclinical randomized controlled multicenter trial (pRCT): anti-CD49d treatment for acute brain ischemia. Sci. Transl. Med. 7, 1–10.

Luong, T.N., Carlisle, H.J., Southwell, A., Patterson, P.H., 2011. Assessment of motor balance and coordination in mice using the balance beam. J. Vis. Exp. 49. https://doi.org/10.3791/2376.

Ma, Y., Shaik, M.A., Kim, S.H., Kozberg, M.G., Thibodeaux, D.N., Zhao, H.T., Yu, H., Hillman, E.M.C., 2016. Wide-field optical mapping of neural activity and brain haemodynamics: considerations and novel approaches. Philos. Trans. R. Soc. Lond. B Biol. Sci. 371. https://doi.org/10.1098/rstb.2015.0360.

Ma, Y., Shaik, M.A., Kozberg, M.G., Kim, S.H., Portes, J.P., Timerman, D., Hillman, E.M.C.. Resting-state hemodynamics are spatiotemporally coupled to synchronized and symmetric neural activity in excitatory neurons. n.d. https://doi.org/10.1073/pnas.1525369113.

Matsui, T., Murakami, T., Ohki, K., 2016. Transient neuronal coactivations embedded in globally propagating waves underlie resting-state functional connectivity. Proc. Natl. Acad. Sci. U.S.A. 113, 6556–6561. https://doi.org/10.1073/pnas.1521299113.

Mcgirr, A., Ledue, J., Chan, A.W., Xie, Y., Murphy, T.H., Murphy, T., Muenchen, U., 2017. Cortical functional hyperconnectivity in a mouse model of depression and selective network effects of ketamine-functional-hyperconnectivity-in-a-mouse. Brain 140, 2210–2225. https://doi.org/10.1093/brain/awx142.

McKeown, M.J., Makeig, S., Brown, G.G., Jung, T., Kindermann, S.S., Bell, A.J., Sejnowski, T.J., 1998. Analysis of fMRI data by blind separation into independent spatial components. Hum. Brain Mapp. 6, 160–188. https://doi.org/10.1002/(SICI)1097-0193(1998)6:3<160::AID-HBM5>3.0.CO;2-1.

Michael, A.M., Anderson, M., Miller, R.L., AdalÄ±, T., Calhoun, V.D., 2014. Preserving subject variability in group fMRI analysis: performance evaluation of GICA vs. IVA. Front. Syst. Neurosci. 8, 1–18. https://doi.org/10.3389/fnsys.2014.00106.

Mohajerani, M.H., Mcvea, D.A., Fingas, M., Murphy, T.H., 2010. Mirrored bilateral slow-wave cortical activity within local circuits revealed by fast bihemispheric voltage-sensitive dye imaging in anesthetized and awake mice. J. Neurosci. 30 (10), 3745–3751. https://doi.org/10.1523/JNEUROSCI.6437-09.2010.

Murase, N., Duque, J., Mazzocchio, R., Cohen, L.G., 2004. Influence of interhemispheric interactions on motor function in chronic stroke. Ann. Neurol. 55, 400–409. https://doi.org/10.1002/ana.10848.

Nasrallah, F.A., Tay, H.C., Chuang, K.H., 2014. Detection of functional connectivity in the resting mouse brain. Neuroimage 86, 417–424. https://doi.org/10.1016/j.neuroimage.2013.10.025.

Orsini, F., Villa, P., Parrella, S., Zangari, R., Zanier, E.R., Gesuete, R., Stravalaci, M., Fumagalli, S., Ottria, R., Reina, J.J., Paladini, A., Micotti, E., Ribeiro-Viana, R., Rojo, J., Pavlov, V.I., Stahl, G.L., Bernardi, A., Gobbi, M., De Simoni, M.G., 2012. Targeting mannose-binding lectin confers long-lasting protection with a surprisingly wide therapeutic window in cerebral ischemia. Circulation 126, 1484–1494. https://doi.org/10.1161/CIRCULATIONAHA.112.103051.

Rehme, A.K., Fink, G.R., Von Cramon, D.Y., Grefkes, C., 2011 Apr. The role of the contralesional motor cortex for motor recovery in the early days after stroke assessed with longitudinal fMRI. Cerebr. Cortex 21 (4), 756–768. https://doi.org/10.1093/cercor/bhq140.

Rubinov, M., Sporns, O., 2011. Weight-conserving characterization of complex functional brain networks. Neuroimage 56, 2068–2079. https://doi.org/10.1016/J.NEUROIMAGE.2011.03.069.

Schindelin, J., Rueden, C.T., Hiner, M.C., Eliceiri, K.W., 2015. The ImageJ ecosystem: an open platform for biomedical image analysis. Mol. Reprod. Dev. 82, 518–529. https://doi.org/10.1002/mrd.22489.

Schroeter, A., Schlegel, F., Seuwen, A., Grandjean, J., Rudin, M., 2014. Specificity of stimulus-evoked fMRI responses in the mouse: the influence of systemic physiological changes associated with innocuous stimulation under four different anesthetics. Neuroimage 94, 372–384. https://doi.org/10.1016/j.neuroimage.2014.01.046.

Silasi, G., Murphy, T.H., 2014. Stroke and the connectome: how connectivity guides therapeutic intervention. Neuron 83, 1354–1368. https://doi.org/10.1016/j.neuron.2014.08.052.

Silasi, G., Xiao, D., Vanni, M.P., Chen, A.C.N., Murphy, T.H., 2016. Intact skull chronic windows for mesoscopic wide-field imaging in awake mice. J. Neurosci. Methods 267, 141–149. https://doi.org/10.1016/j.jneumeth.2016.04.012.

Smith, S.M., Fox, P.T., Miller, K.L., Glahn, D.C., Mickle Fox, P., Mackay, C.E., Filippini, N., Watkins, K.E., Toro, R., Laird, A.R., Beckmann, C.F., 2009. Correspondence of the brain's functional architecture during activation and rest. Proc. Natl. Acad. Sci. Unit. States Am. 106, 13040–13045.

Trueman, R.C., Diaz, C., Farr, T.D., Harrison, D.J., Fuller, A., Tokarczuk, P.F., Stewart, A.J., Paisey, S.J., Dunnett, S.B., 2017. Systematic and detailed analysis of behavioural tests in the rat middle cerebral artery occlusion model of stroke: tests for long-term assessment. J. Cereb. Blood Flow Metab. 37, 1349–1361. https://doi.org/10.1177/0271678X16654921.

Urbin, M.A., Hong, X., Lang, C.E., Carter, A.R., 2014. Resting-state functional connectivity and its association with multiple domains of upper-extremity function in chronic stroke. Neurorehabilitation Neural Repair 28, 761–769. https://doi.org/10.1177/1545968314522349.

Van Meer, M.P.A., Van Der Marel, K., Wang, K., Otte, W.M., Bouazati, S. El, Roeling, T.A.P., Viergever, M.A., Berkelbach Van Der Sprenkel, J.W., Dijkhuizen, R.M., 2010. Recovery of sensorimotor function after experimental stroke correlates with restoration of resting-state interhemispheric functional connectivity. J. Neurosci. 30 (11), 3964–3972. https://doi.org/10.1523/JNEUROSCI.5709-09.2010.

Vanni, M.P., Chan, A.W., Balbi, M., Silasi, G., Murphy, T.H., 2017. Mesoscale mapping of mouse cortex reveals frequency-dependent cycling between distinct macroscale functional modules. J. Neurosci. 37, 7513–7533. https://doi.org/10.1523/JNEUROSCI.3560-16.2017.

Vanni, M.P., Murphy, T.H., 2014. Mesoscale transcranial spontaneous activity mapping in GCaMP3 transgenic mice reveals extensive reciprocal connections between areas of somatomotor cortex. J. Neurosci. 34 (48), 15931–15946. https://doi.org/10.1523/JNEUROSCI.1818-14.2014.

Ward, N.S., Brown, M.M., Thompson, A.J., Frackowiak, R.S.J., 2003. Neural correlates of motor recovery after stroke: a longitudinal fMRI study. Brain 126, 2476–2496. https://doi.org/10.1093/brain/awg245.

Wright, P.W., Brier, L.M., Bauer, A.Q., Baxter, G.A., Kraft, A.W., Reisman, M.D., Bice, A.R., Snyder, A.Z., Lee, J.-M., Culver, J.P., 2017. Functional connectivity structure of cortical calcium dynamics in anesthetized and awake mice. PLoS One 12, e0185759. https://doi.org/10.1371/journal.pone.0185759.

Zerbi, V., Grandjean, J., Rudin, M., Wenderoth, N., 2015. Mapping the mouse brain with rs-fMRI: an optimized pipeline for functional network identification. Neuroimage 123, 11–21. https://doi.org/10.1016/j.neuroimage.2015.07.090.